EVALUATION AND MITIGATION OF RESIDUAL MAGNETIC FIELD FROM THE HIGH-VOLTAGE PULSE POWER SUPPLY FOR THE BEAM KICKER IN THE MUON G-2/EDM EXPERIMENT

Y. Kawase*, S. Narita, R. Hosokawa, Iwate University, Japan
H. Iinuma, H. Sato, Ibaraki University, Japan
S. Ogawa, T. Mibe, High Energy Accelerator Research Organization, Tsukuba, Japan
T. Takayanagi, Japan Atomic Energy Agency, Tokai, Japan
R. Matsushita, T. Mibe, The University of Tokyo, Tokyo, Japan
T. Yamanaka, Kyushu University, Fukuoka, Japan

Abstract

In the J-PARC muon $g-2$/EDM experiment, precise control of the muon beam is essential to achieve the required measurement accuracy. For this purpose, the development of a new high-voltage and high-current pulse power supply (kicker power supply) is indispensable. Because the accuracy of the $g-2$ measurement strongly depends on the uniformity of the magnetic field, and the muon beam must remain confined within a region of ± 5 cm in height and a radius of 33.3 cm, any residual magnetic field leads to a degradation of the precision. While the design of the static magnetic field is being developed to meet the experimental requirements, the residual dynamic magnetic field remains a challenge. In this study, aiming to develop a power supply that satisfies the required precision, we evaluated the impact of the residual magnetic field caused by the kicker power supply on the measurement accuracy. This paper reports the evaluation results and our future plans to reduce the residual magnetic fields.

INTRODUCTION

The Standard Model describes elementary particle interactions with high precision, but phenomena such as dark matter and baryon asymmetry remain unexplained, motivating searches for physics beyond the Standard Model (BSM).

The anomalous magnetic moment of the muon ($g-2$) is a powerful probe of BSM physics due to its high theoretical and experimental precision. Previous measurements at BNL [1] and FNAL [2] employed similar techniques, leaving the possibility of common systematic uncertainties.

The J-PARC muon $g-2$/EDM experiment adopts a different approach, using a compact storage ring with an ultra-low emittance beam and no electric field focusing [3]. By employing a three-dimensional spiral injection, it provides an independent measurement with a distinct systematic uncertainty [4], aiming at 0.45 ppm (stat.) with < 0.1 ppm (syst.).

THREE-DIMENSIONAL SPIRAL INJECTION AND KICKER SYSTEM

A μ^+ beam with a momentum of 300 MeV/c is injected obliquely downward from the upper edge of the storage magnet and follows a spiral trajectory while moving downward, wrapping around the main magnetic field of approximately 3 T applied inside the storage magnet (Fig. 1). After injection, the beam is guided by the kicker magnetic field and the weak focusing magnetic field, and subsequently oscillates within a limited region around a certain plane in the storage magnet (the storage plane). The muons then circulate stably in a nearly circular orbit until they decay.

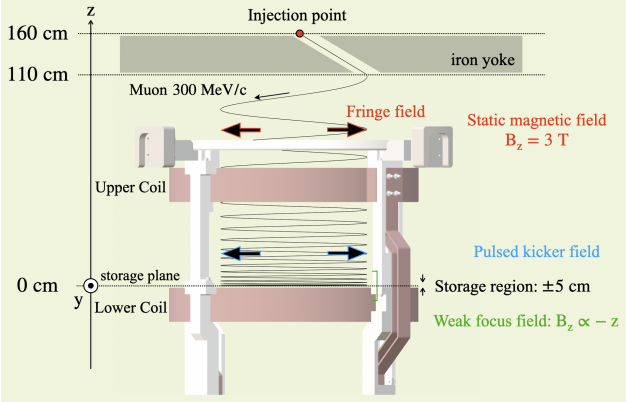

Figure 1: Concept of three-dimensional beam injection.

The weak focusing magnetic field [4, 5] is described by

$$B_r = -n\frac{B_0}{r_0}z, \quad B_z = B_0\left[1 - n\frac{r-r_0}{r_0} + \frac{n}{2}\left(\frac{z}{r_0}\right)^2\right],$$

where B_r and B_z are the radial and axial magnetic field components, respectively, r and z denote the radial and vertical positions, and $B_0 = 3$ T and $r_0 = 33.3$ cm. The field was implemented using the field index n ($= 1.5 \times 10^{-4}$). This weak focusing field induces vertical betatron oscillations (VBO), causing the stored muon beam to oscillate vertically around the storage plane with a period of approximately 600 ns.

The kicker magnetic field is generated by applying a pulsed current from pulse power supplies (kicker power supplies) to single-turn coils (kicker coils) placed above and below the storage region. As shown in Fig. 2, the current waveform delivered from the kicker power supply to the kicker coil can be categorized according to the kick timing and detector operation timing into three regions: the main pulse, the pulse-end region, and the fit range.

To achieve the target physics measurement precision and to confine the muon beam within the storage acceptance of

* s3125003@iwate-u.ac.jp

±5 cm, the kicker coil must be driven by a half-sine current pulse with a peak current of 1 kA, a pulse width of 120 ns, and a repetition rate of 25 Hz. In addition, instabilities at the pulse end, such as ringing, undershoot, and residual current, must be sufficiently suppressed.

However, in practice, it is difficult to completely eliminate these residual currents. In particular, reflections and resonances arising from the inductive and capacitive components of the load (LC characteristics) make suppression challenging. Furthermore, since the stored beam remains within the kicker field region, even small residual magnetic fields can repeatedly affect the beam and accumulate over time, imposing strict requirements on pulse-end stability.

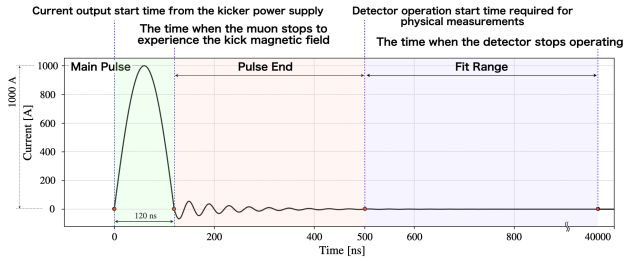

Figure 2: Explanation of current waveform from kicker power supply.

Residual currents generate additional magnetic fields that affect the measurement through two mechanisms. The vertical component (B_z) directly modifies the spin precession frequency ($\omega_a \propto |\vec{B}|$), while the radial component (B_r) changes the VBO amplitude and thus the effective B_z experienced by the muons. As a result, both lead to deviations in ω_a and degrade the measurement precision.

In this study, we evaluate the impact of pulse-end current instabilities in the current waveform supplied from the kicker power supply to the kicker coil on the measurement precision. Based on this evaluation, we discuss criteria for determining the required specifications of the kicker power supply.

SIMULATION METHOD

A Geant4 [6]-based simulation was performed to evaluate the impact of residual kicker current on the muon spin precession measurement. The simulation was carried out using single-particle tracking, with initial conditions set to an ideal orbit with VBO = 0 cm. The trajectory of each injected particle was tracked after reaching the storage plane, and both the momentum vector $\vec{p}$ and spin vector $\vec{s}$ were recorded as a function of time. As a validation of the tracking simulation, we confirmed that, in the absence of residual magnetic-field perturbations, the relative variation of the momentum magnitude remained at the level of 10^{-6}, demonstrating sufficient numerical stability for the present study.

The anomalous precession frequency $\vec{\omega}_a$, defined as the difference between the spin precession and cyclotron frequencies, is given by

$$\vec{\omega}_a = -\frac{q}{m}\left[a_\mu \vec{B} - \left(a_\mu - \frac{1}{\gamma^2 - 1}\right)\frac{\vec{\beta} \times \vec{E}}{c}\right]. \quad (1)$$

Here, $\vec{\beta} = \vec{v}/c$ and γ is the Lorentz factor. Since no electric field is applied in the present study, the second term can be neglected. The spin precession was evaluated by calculating

$$\cos\theta = \frac{\vec{p} \cdot \vec{s}}{|\vec{p}|\,|\vec{s}|}.$$

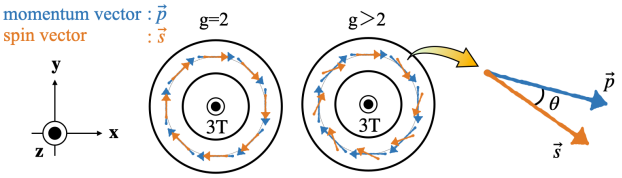

Figure 3: Relation between the momentum and spin vectors.

As shown in Fig. 3, if $g = 2$, the spin precesses at the same frequency as the momentum, and therefore the angle between $\vec{p}$ and $\vec{s}$ remains zero. In contrast, if $g > 2$, the spin precesses faster than the momentum, leading to a non-zero relative angle. The time dependence of this angle reflects the anomalous precession frequency ω_a. The time dependence of $\cos\theta$ was fitted with

$$f(t) = \cos(\omega_a t + \phi_a),$$

to extract the anomalous spin precession frequency ω_a. For simplicity, the phase ϕ_a was set to zero in this study. To account for the muon decay, an exponential weight was applied in the fitting procedure:

$$w(t) \propto e^{-t/(\gamma\tau)},$$

where γ is the Lorentz factor and $\tau \approx 2.2\,\mu$s is the muon lifetime. The extracted ω_a was compared with the reference value $\omega_{a,\mathrm{default}}$ obtained without residual current effects. The difference,

$$\Delta\omega_a = \omega_a - \omega_{a,\mathrm{default}}, \quad (2)$$

was evaluated as a measure of systematic bias. From Eqs. (1) and (2), any deviation $\Delta\omega_a$ directly corresponds to a degradation of the $g-2$ measurement precision.

In this study, the residual current in the pulse-end region was classified into three components: ringing, undershoot, and a DC component. The impact of each component on the physics measurement precision was evaluated separately.

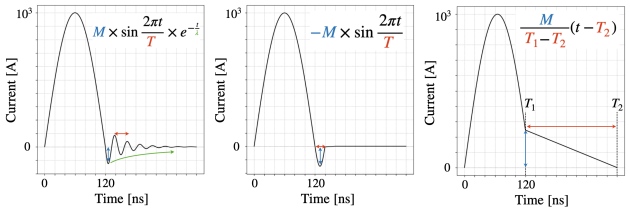

Figure 4: Residual current components in the pulse-end region and fit range: (left) ringing, (center) undershoot, and (right) DC component.

Each residual current component was modeled using the functional forms shown in Fig. 4. By varying the parameters corresponding to the amplitude, pulse width, and decay time constant in each function, the influence of different residual current shapes was systematically investigated.

EVALUATION OF THE IMPACT

In this study, as shown in Fig. 4, the ringing in the pulse-end region was modeled by a damped sinusoidal function. M is the amplitude normalized to the main pulse, T is the ringing period, and λ is the decay time constant. These parameters were set in the following ranges: M = 1–100 A, T = 10–2000 ns, and λ up to ∞, where $\lambda = \infty$ represents the upper limit corresponding to no decay.

Figure 5 (left) shows the dependence of $\Delta\omega_a/\omega_a$ on the ringing period and amplitude. A pronounced deviation is observed when the ringing period approaches the VBO period. This behavior suggests a resonance-like enhancement between the residual magnetic field and the VBO motion. Figure 5 (right) shows the impact of varying the VBO period on the peak position of $\Delta\omega_a/\omega_a$. This result supports the interpretation that the resonance between the ringing and the VBO motion enhances the systematic error. In Figure 5 (left), the yellow line indicates the target precision boundary of 0.1 ppm. It is found that when the ringing period is shorter than approximately 200 ns, the target $g-2$ measurement precision can be maintained if the ringing amplitude is suppressed below 1% of the main pulse amplitude, corresponding to less than 10 A.

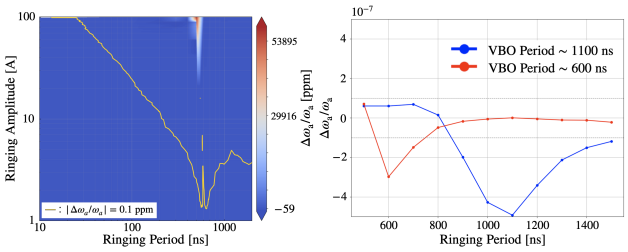

Figure 5: (Left) Impact of ringing on the measurement precision. (Right) Dependence of $\Delta\omega_a/\omega_a$ on the VBO period.

The undershoot component in the pulse-end region was modeled as a negative half-sine function, M is the amplitude of undershoot and T is the undershoot period. The parameter scan was performed over the ranges M = 1–100 A and T = 10–2000 ns.

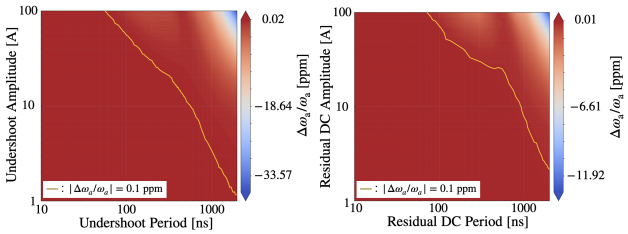

Figure 6: Impact on the physics measurement precision: (Left) Undershoot, (Right) DC component.

Figure 6 (left) shows the dependence of $\Delta\omega_a/\omega_a$ on the undershoot period and amplitude. As the undershoot amplitude or period increases, the total integrated magnetic field increases, modifying the stored muon trajectory and leading to a systematic shift in ω_a. In particular, the impact is smaller than ringing since it corresponds to a single kick. In Figure 6 (left), the yellow line indicates the target precision boundary of 0.1 ppm. It is confirmed that when the undershoot period is shorter than approximately 600 ns, the target $g-2$ measurement precision can be maintained by suppressing the undershoot amplitude below 1% of the main pulse amplitude (i.e., less than 10 A).

The residual DC component was modeled as a linearly decaying function, M is the amplitude of residual DC and T_1, T_2 define the duration of the residual current. The parameter scan was performed for M = 1–100 A and pulse widths ranging from 10 ns to 2000 ns.

Figure 6 (right) shows the dependence of $\Delta\omega_a/\omega_a$ on the residual-current duration and amplitude. As the amplitude or duration increases, the total integrated magnetic field becomes larger, resulting in a modification of the stored orbit and a systematic shift in ω_a. As can be seen from the figure, the trends of the 0.1 ppm boundary for the undershoot and residual DC components are similar. This is because an increase in the pulse width leads to a larger residual magnetic field, resulting in a modification of the stored orbit, and hence a similar impact on the systematic error.

SUMMARY AND FUTURE WORK

We evaluated the impact of pulse-end residual currents in the kicker power supply on the muon $g-2$ measurement precision using a Geant4-based simulation. The residual current was classified into three components: ringing, undershoot, and residual DC current.

For ringing, a significant shift in ω_a was observed when the ringing period approached the vertical betatron oscillation (VBO) period, indicating a resonance-like coupling with the beam motion. The target precision can be maintained when the ringing period is shorter than approximately 200 ns and the amplitude is suppressed below 1% of the main pulse amplitude (i.e., less than 10 A). For undershoot, the impact is smaller than that of ringing because it corresponds to a single kick, and depends on the phase relative to the VBO motion. The target precision can be maintained when the undershoot period is shorter than approximately 600 ns and the amplitude is below 1%. The residual DC component produces a systematic shift that increases with amplitude and duration due to the larger integrated magnetic field. A similar trend to the undershoot case is observed for the 0.1 ppm boundary. These results provide practical design constraints for the kicker power supply.

As a next step, we plan to design and implement a combined passive and active compensation circuit based on a noise-cancellation concept, in which an inverse-phase current is generated to suppress pulse-end components. Passive circuits alone can suppress residual currents, but their performance strongly depends on the LC characteristics of the load, requiring circuit redesign for different conditions.

REFERENCES

[1] G. W. Bennett *et al.*, "Final report of the Muon E821 anomalous magnetic moment measurement at BNL," *Phys. Rev. D*, vol. 73,

p. 072003, 2006. doi:10.1103/PhysRevD.73.072003

[2] D. P. Aguillard *et al.*, "Measurement of the positive muon anomalous magnetic moment to 127 ppb," *Phys. Rev. Lett.*, vol. 135, p. 101802, 2025. doi:10.1103/7clf-sm2v

[3] M. Abe *et al.*, "A new approach for measuring the muon anomalous magnetic moment and electric dipole moment," *Prog. Theor. Exp. Phys.*, vol. 2019, p. 053C02, 2019. doi:10.1093/ptep/ptz030

[4] H. Iinuma *et al.*, "Three-dimensional spiral injection scheme for the $g-2$/EDM experiment at J-PARC," *Nucl. Instrum. Methods Phys. Res. A*, vol. 832, pp. 51–62, 2016. doi:10.1016/j.nima.2016.05.126

[5] M. Abe *et al.*, "Magnetic design and method of a superconducting magnet for muon $g-2$/EDM precise measurements in a cylindrical volume with homogeneous magnetic field," *Nucl. Instrum. Methods Phys. Res. A*, vol. 890, pp. 51–63, 2018. doi:10.1016/j.nima.2018.01.026

[6] S. Agostinelli *et al.*, "Geant4—a simulation toolkit," *Nucl. Instrum. Methods Phys. Res. A*, vol. 506, pp. 250–303, 2003. doi:10.1016/S0168-9002(03)01368-8